Direct Evidence of Lipid Rafts by in situ Atomic Force Microscopy

Mingjun Cai, Weidong Zhao, Xin Shang, Junguang Jiang, Hongbin Ji, Zhiyong Tang, and Hongda Wang**

Lipid rafts are membrane microdomains enriched with cholesterol, glycosphingolipids, and proteins. Although they are broadly presumed to play a pivotal role in various cellular functions, there are still fierce debates about the composition, functions, and even existence of lipid rafts. Here high-resolution and time-lapse in situ atomic force microscopy is used to directly confirm the existence of lipid rafts in native erythrocyte membranes. The results indicate some important aspects of lipid rafts: most of the lipid rafts are in the size range of 100–300 nm and have irregular shape; the detergent-resistant membranes consist of cholesterol microdomains and are not likely the same as the lipid rafts; cholesterol contributes significantly to the formation and stability of the protein domains; and Band III is an important protein of lipid rafts in the inner leaflet of erythrocyte membranes, indicating that lipid rafts are exactly the functional domains in plasma membrane. This work provides direct evidence of the presence, size, and main constitutive protein of lipid rafts at a resolution of a few nanometers, which will pave the way for studying their structure and functions in detail.

1. Introduction

The plasma membrane mainly consists of phospholipids, glycolipid, cholesterol, and proteins that are dynamic and not homogeneously distributed within the bilayer.[1,2] Many studies have revealed that the molecules in cell membranes tend to organize into microdomains termed "lipid rafts", in which cholesterol, sphingolipid, and specific membrane proteins are enriched.[3,4] Lipid rafts are broadly presumed to play an important role in various cell functions (e.g., signal transduction,[5,6] endocytosis,[7] and virus infection[8,9]) and to be associated with actin cytoskeletons to fulfill their proper functions.[10]

The major characteristics of lipid rafts have been originally inferred from detergent-resistant membranes (DRMs). Generally, DRMs can be prepared by the cold extraction of plasma membranes with nonionic detergents. Though different detergents result in DRMs with different compositions,[11] Triton X-100 is a commonly used reagent to prepare them.[12] The traditional definition of lipid rafts is the membrane domains that are resistant to extraction by Triton X-100 at 4 °C and float in the upper half of sucrose density gradient centrifugation.[13] However, whether or not DRMs are real representations of the organization of lipid rafts in plasma membranes is still a subject of debate.[14–16] Experimental results about the model membranes have borne out evidence on the crucial role of cholesterol in detergent resistance.[17,18] The high concentration of cholesterol in the plasma membranes is likely responsible for the insolubility of DRMs in detergent solution.

M. Cai,[+] W. Zhao,[+] X. Shang, Dr. J. Jiang, Prof. H. Wang
State Key Laboratory of Electroanalytical Chemistry
Changchun Institute of Applied Chemistry
Chinese Academy of Sciences, Changchun
Jilin 130022, PR China
E-mail: hdwang@ciac.jl.cn

W. Zhao
Graduate University of Chinese Academy of Sciences
Beijing 100049, PR China

Prof. H. Ji
State Key Laboratory of Cell Biology
Institute of Biochemistry and Cell Biology
Shanghai Institutes of Biological Sciences
Shanghai 200032, PR China

Prof. Z. Tang
National Center for Nanoscience and Technology
Beijing 100190, PR China
E-mail: zytang@nanoctr.cn

[+] M.C. and W.Z. contributed equally to this work.

DOI: 10.1002/smll.201102183

Lipid rafts are dynamic and heterogeneous so that it is difficult to find a universal approach to study them. The uncertain microdomains of lipid rafts are too small to be observed by light microscopy.[19,20] Traditional assays such as sucrose density gradient centrifugation, electrophoresis, fluorescence staining, and electron microscopy may destroy the structure of lipid rafts. Although the nanoscale dynamics of lipids in the living cell was successfully detected by stimulated emission depletion (STED) far-field fluorescence nanoscopy,[21] labeling the lipids with fluorescent dye and using a high power donut laser (up to 380 mW) may be not suitable to provide the whole picture of lipid rafts.

Atomic force microscopy (AFM), a key family member of scanning probe microscopy, may offer a solution to in situ imaging of lipid rafts without large structural perturbations. AFM takes advantage of a microfabricated cantilever with a sharp tip to scan the surface of the samples, and the deflection of the cantilever is utilized to record the information of the surface properties. AFM allows imaging of cellular membranes at a spatial resolution of a few nanometers.[22,23] One of the greatest advantages of AFM is that it can image the samples in solutions under ambient conditions, which makes it very important in biological applications.[24] Furthermore, recent advances in AFM technique extend its application to recognize specific molecules in heterogeneous samples at the single-molecule level, which is called topography and recognition imaging (TREC).[22,25,26] TREC scans a sample with an antibody-attached AFM tip. A topographic image is generated simultaneously with a recognition image that exactly locates the binding sites of antigen and antibody, leading to positioning of the individual molecules within the topographic image. The recognition process is efficient, specific, and reproducible.

AFM has been employed to study lipid rafts based on model membranes that are mainly composed of 1,2-dipalmitoyl-*sn*-glycero-3-phosphocholine (DPPC), 1,2-dioleoyl-*sn*-glycero-3-phosphocholine (DOPC), 1-palmitoyl-2-oleoyl-*sn*-glycero-3-phosphochline (POPC) and cholesterol. Real-time AFM directly imaged the change of the model membranes treated with Triton X-100 at the nanometer level, which indicates that AFM is a unique tool to investigate the structure of biological membranes in situ.[27] Unfortunately, there are almost no proteins in the artificial model membranes. Therefore these results only confirm that the DRMs exist in model membranes, and the cholesterol is related to the rigidity in lipid bilayers.[18] Though the study of lipid rafts of mammalian cell membranes by AFM has been reported, the plasma membrane was not prepared under physiological conditions and so the high-resolution and in situ imaging of the corresponding lipid rafts has not yet been achieved.[28]

Herein, the lipid rafts from human erythrocytes were selected for investigation by in situ AFM. The human erythrocytes that lack intracellular organelles are an ideal model for the study of biological membranes. Though there are several reports on the isolation of DRMs from human erythrocytes and characterization of DRMs, none of these studies is carried out under physiological conditions.[29,30] We used AFM to monitor in situ the vanishing process of cholesterol microdomains treated with methyl-β-cyclodextrin (MβCD), and study the resistance of microdomains of native erythrocyte membranes to Triton X-100 under physiological conditions. We directly confirm the existence of lipid rafts in the erythrocyte membranes at high resolution, and reveal the relationship between the erythrocyte anion transporter, Band III, and the lipid raft microdomains.

2. Results

2.1. Observation of the Outer and Inner Leaflet of Cell Membranes under Native Conditions

To obtain the outer and inner leaflet membranes in native states, erythrocytes were deposited onto aminopropyltriethoxysilane modified mica (APTES-mica) substrates, and subsequently the erythrocytes were sheared open by a stream of low-concentration ionic buffer solution as described in the Experimental Section. The prepared membranes were imaged in PBS by Acoustic AC (AAC) mode AFM at room temperature. The mica was chosen to attach the washed erythrocytes, because it has atomic flat surface and attaches the membranes only through the electrostatic interaction, and correspondingly has a minimum effect on the structure of cell membranes.[22] Modifying mica surface with APTES might offer sufficient amino functional groups to attach the membrane tightly. Without the APTES modification, the mica and glass could not attach to the membranes stably.[22]

Figure 1A represents a typical image of the outer leaflet membrane of flat erythrocyte ghosts—the intact erythrocyte membranes without the soluble proteins and membrane skeletons[31]—that were uniformly distributed on the APTES-mica, indicating that the bottom layer of erythrocyte ghosts was attached onto the surface tightly. The outer leaflet membranes are flat and rather smooth. The average diameters of the membranes are about 8 μm, which is very close to the size of whole erythrocytes. The average heights of the erythrocyte ghosts were measured to be about 20 nm, which suggests that two layers of cell membranes were overlapped, since the height of single layer of cell membranes is about 10 nm.[22]

Figure 1B shows the topographic image of the inner leaflet of erythrocyte membranes prepared by shearing the

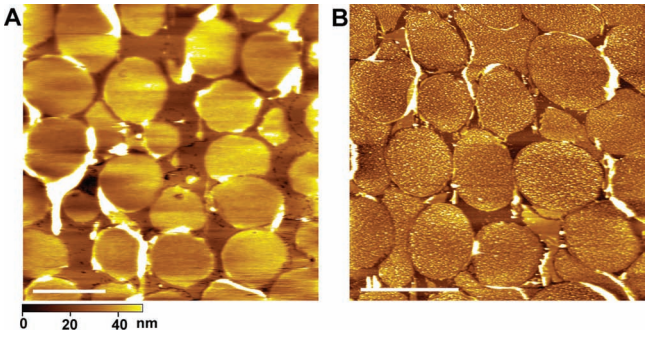

Figure 1. AFM images of the outer and inner leaflet of cell membranes on APTES-mica in PBS. The outer leaflet membrane (A) is smooth, while the inner leaflet membrane (B) is rough with plenty of proteins. The average diameter of cell membranes is about 8 μm. Scale bars are 10 μm.

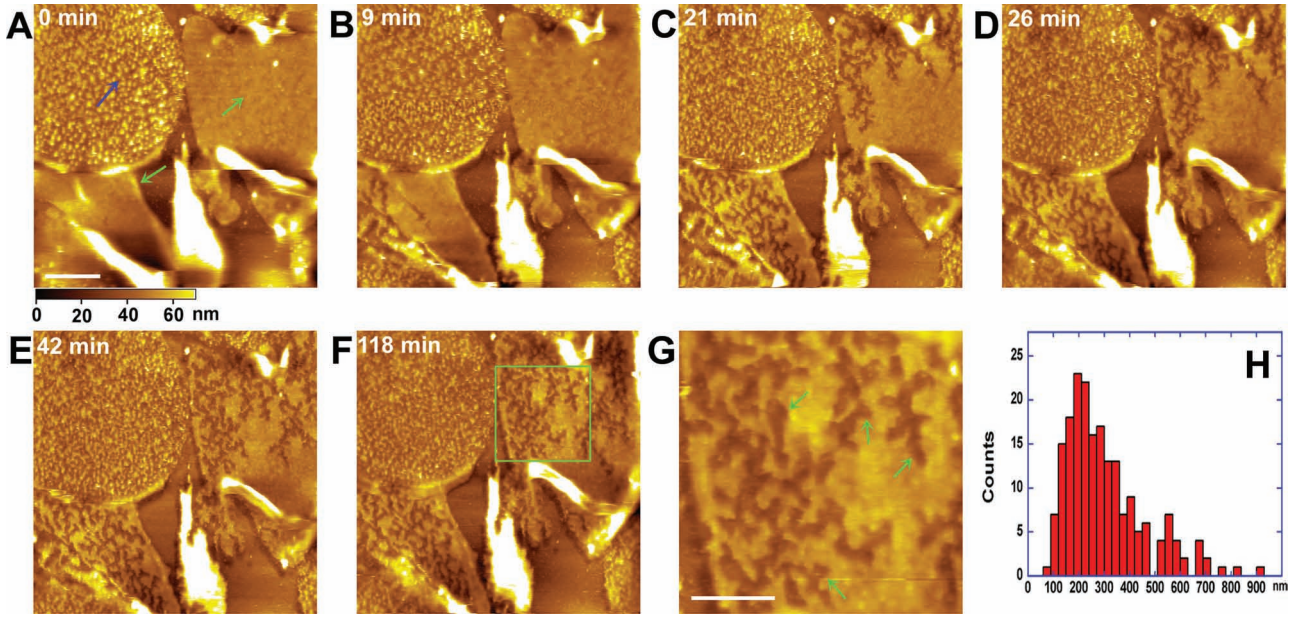

Figure 2. Real-time images of cell membranes treated with MβCD. A–F) Series of images after the addition of MβCD for 0 (A), 9 (B), 21 (C), 26 (D), 42 (E) and 118 (F) min. The green and blue arrows in (A) point to the outer and inner leaflets of cell membranes, respectively. G) High resolution image of the green square area in (F), in which the green arrows indicate the regions eroded by the MβCD. H) Size distribution of the regions of the outer leaflet membrane eroded by the MβCD in Figure 2F. Scale bars: 2 μm in (A), 1 μm in (G).

erythrocytes. Evidently, the inner leaflet membranes with dense proteins are rough and quite different from the outer leaflet membranes, which is in agreement with our previous studies.[32] The heights of the inner leaflet membrane are about 10 nm, half of those of the ghost membranes in Figure 1A.

2.2. Erythrocyte Membranes Treated with MβCD in situ

The extraction of cholesterol from membranes is the main way to disrupt lipid rafts. MβCD is the most widely used reagent to extract cholesterol from both the plasma membranes and model membranes, as the cavity of the MβCD is hydrophobic and the size of the cavity is suitable to accommodate cholesterol.[33–35] MβCD works as a type of solvent to extract the cholesterol rather than insert in the lipid bilayer, so MβCD has the minimum effect on the structure of the lipid bilayer domain without cholesterol.

In order to observe the in situ interaction between MβCD and erythrocyte membranes directly, 2 mM MβCD was injected into the AFM sample chamber, and serial real-time AFM images in the same area were recorded to monitor the changes. As shown in **Figure 2**A, in the same image there are both outer and inner leaflet membranes, indicated by green and blue arrows, respectively. After the injection of MβCD, the change was revealed by real-time AFM immediately. At 9 min (Figure 2B), the crevices appeared on the outer leaflet membrane at the bottom left part of the image; however, the inner leaflet membrane (at the top left part) experienced no significant changes. Subsequently, the outer leaflet reacted with MβCD gradually and became branched membranes, as shown in the bottom left and top right corner in Figure 2C and D (corresponding to 21 and 26 min after the addition of MβCD, respectively). The inner leaflet still showed no significant changes in the topographic image but depletion of some proteins. The effect of MβCD on the outer leaflet membrane became less obvious with prolonging time (Figure 2F, 118 min). The heights of both the outer and inner leaflet membranes decreased because some proteins in the membranes were eliminated. Figure 2G is a magnified image of the green square area in Figure 2F. The indentations indicated by the green arrows were eroded positions caused by the MβCD. Figure 2H is the size distribution of these indentations, which shows that 60% of the indentations eroded by MβCD are 100–300 nm. These sizes may be a bit larger than the size of lipid rafts measured by other methods,[36] possibly due to the elimination of neighboring proteins when the lipid rafts were disrupted.

2.3. The Digested Inner Leaflet of Cell Membranes Treated with MβCD

To study the effect of proteins on the resistance of the inner cell membrane to MβCD, we digested the inner membrane proteins first using trypsin, and then monitored the changes after addition of MβCD. As shown in **Figure 3**A, the inner leaflet membrane is smooth and flat after the digestion of the embedded proteins by trypsin for 1 h. The height of the digested membrane decreased from around 10 to 4 nm due to the protein removal. After 2 mM MβCD was injected into the AFM sample chamber, the images were recorded using real-time AFM (Figure 3B). The membranes reacted with MβCD quickly. Figure 3C represents the magnified image of the green square area in Figure 3B. The small particles pointed by

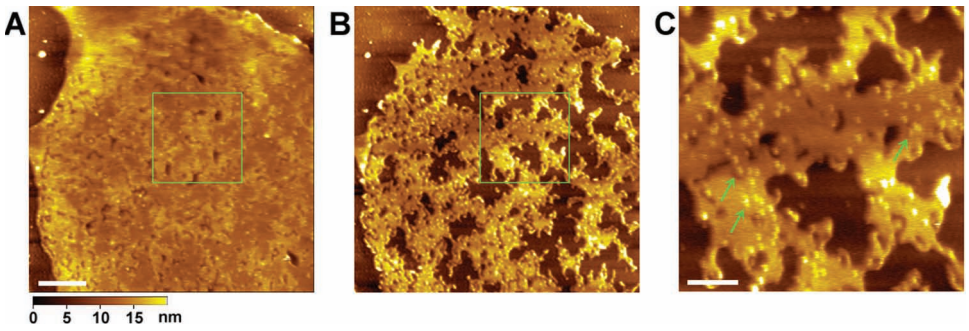

Figure 3. In situ AFM images of the digested inner leaflet membrane treated with MβCD. A) The inner leaflet membrane after digestion by trypsin (1 mg mL^{-1}) for 1 h at 37 °C. B) The same area in (A) after treatment with 2 mM MβCD. C) Magnified image of the green square area in Figure 3B. The green arrows point to the undigested transmembrane proteins. Scale bars: 1 μm in (A), 300 nm in (C).

the green arrows could be a few undigested transmembrane proteins.[37] The cholesterol depletion by MβCD was to disrupt the connection between the proteins and phospholipids. After membrane proteins were digested by trypsin, the inner leaflet membrane were dissolved quickly, suggesting that the lipid bilayer would show similar features both in the outer and inner leaflet of cell membranes if there were no transmembrane proteins stationed in cell membranes.

2.4. Observation of DRMs in situ

Triton X-100 is a commonly used biochemical reagent to prepare DRMs. To observe the DRMs in situ, the prepared erythrocyte membranes were incubated with Triton X-100, and then scanned in PBS by AFM. **Figure 4**A shows a topographic image of erythrocyte membranes incubated with 0.1% (v/v) Triton X-100 at 4 °C. Figure 4B and C are gradually magnified images of Figure 4A, in which we can observe the details of DRMs that there are perforated and irregular membrane domains in the whole image. The sizes of DRMs vary from about 50 to 950 nm, and 45% of them are in the range 100 to 200 nm, as depicted in Figure 4D, which is in agreement with the reported size measured by other indirect labeling methods, such as electron microscopy.[36] The height distribution of the membranes is in the range 2 to 4 nm, with the average at about 2.5 nm (as shown in Figure 4E), which is consistent with the measured height of lipid bilayer by AFM[32] but lower than that of the model lipid bilayer measured by other methods, because of tip pressure during imaging.[38] AFM images of DRMs from the erythrocyte membranes were taken in situ. The cracked membranes suggest that some phospholipid bilayers in the erythrocyte membranes can be dissolved by Triton X-100, and there are still membrane domains, i.e., DRMs, resistant to Triton X-100.[30]

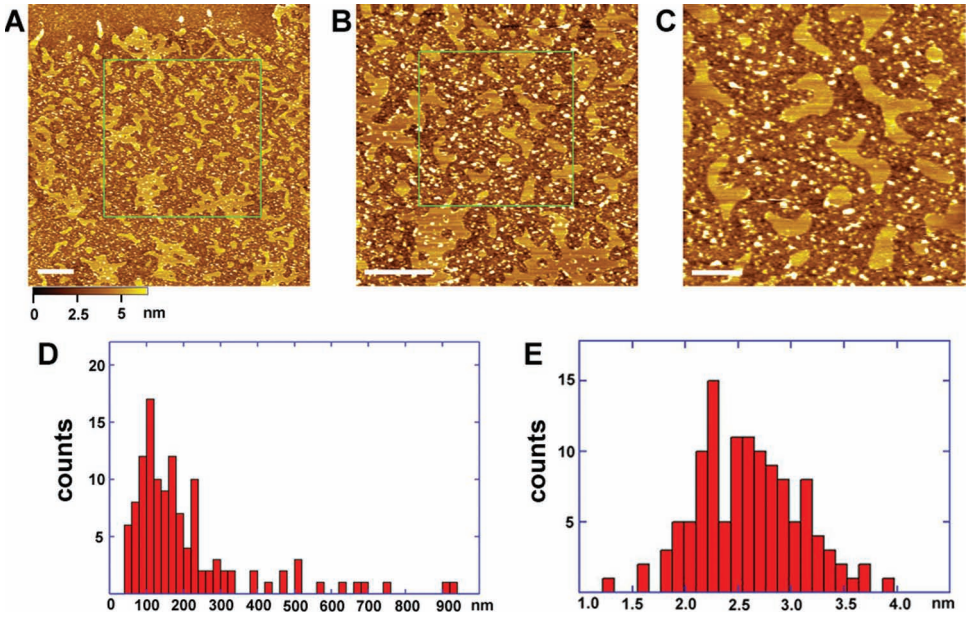

Figure 4. DRMs from the outer leaflet membrane. A) AFM image of DRMs. B, C), Serial magnifications of the DRMs in (A). D, E), Size and height distribution of the DRMs in (A), respectively. Scale bars: 500 nm in (A) and (B), 200 nm in (C).

small NANO MICRO

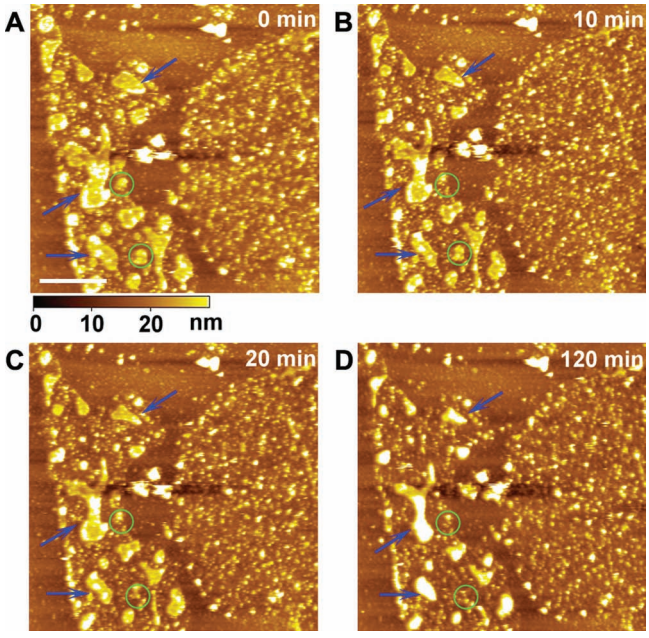

Figure 5. Real-time effects of MβCD on the DRMs of erythrocyte membranes. The images show the different stage after addition of MβCD for 0 (A), 10 (B), 20 (C), and 120 (D) min. The green circles and blue arrows in Figure 5A point to the DRMs that have completely vanished or have been partly diminished, respectively. Scale bar is 1 μm.

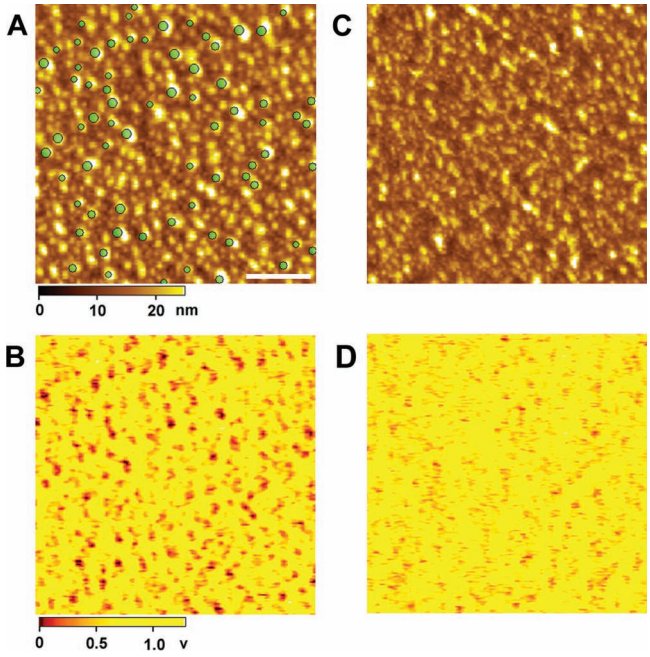

Figure 6. AFM recognition images of the Band III in the inner leaflet membrane. A) Topographic image of the inner leaflet membrane before treatment with 2 mM MβCD. B) Recognition image corresponding to (A). The dark signal represents the recognition event. The recognition signal was superimposed onto the topographic images in Figure 6A (the green dots). C) Topographic image of the inner leaflet membrane after the treatment with 2 mM MβCD. D) Recognition image corresponding to (C). Scale bar is 500 nm.

2.5. DRMs Treated with MβCD

To further investigate the component of DRMs obtained by incubating the membranes with Triton X-100, we treated the DRMs with MβCD.[39] Time-lapse AFM was used to track the real-time change of the DRMs treated with MβCD.

The DRMs, obtained as described in the Experimental Section, are shown in **Figure 5**A. The membranes in the left and right half of Figure 5A are the treated outer and inner leaflet membrane, respectively, which are quite different both in size and in shape. DRMs are clearly observed in the outer leaflet membrane, whereas Triton X-100 has little effect on the inner leaflet membrane. After 2 mM MβCD was injected into the sample chamber, a series of images were recorded by AFM. As shown in Figure 5B–D, in the beginning MβCD dissolved some DRMs in the outer leaflet membrane quickly (about 20 min, as shown in Figure 5C); then, the reaction became slow and gradually less apparent. After 120 min, as shown in Figure 5D, the DRMs did not further react with MβCD. From the serial images, we can clearly observe that different DRMs exhibited different resistance behavior. Some DRMs completely vanished, and others were partly diminished, as indicated by the green circles and blue arrows in Figure 5, respectively. However, there was no obvious change in the inner leaflet membrane over all the time, except for reduction of the height. The results indicate that DRMs consist of cholesterol microdomains, and are likely not the same as the lipid rafts; meanwhile, the DRMs in the outer and inner leaflet membranes show the different effects in reacting with MβCD.

2.6. Recognition Imaging of Band III in the Inner Leaflet Membrane

The erythrocyte anion transporter, Band III, is one of the most important proteins in erythrocyte membranes, and plays an important role in many functions of cells.[40] Though centrifugal separation and flow cytometric analysis have indicated that Band III establishes contact with lipid rafts,[29,41] these methods are indirect and not performed under native conditions. Here we employed the molecular recognition imaging technique to investigate the relationship between the lipid rafts and Band III under physiological buffer conditions.

Figure 6A and B show the topography and recognition images of the inner leaflet membrane, respectively. The spots in Figure 6A represent membrane protein domains with size in the range 100 to 150 nm. The dark spots in Figure 6B are the recognition signal that corresponds to the location of Band III in the membrane. To clearly demonstrate the distribution of Band III in the membrane, we superimposed the recognition signal onto the topographic image (the green dots in Figure 6A), which clearly shows that Band III is just located in the protein domains. It is noted that the sizes of recognition spots are larger than that of single Band III,[42] which indicates that there may be Band III aggregates in the membrane protein domains. To clarify the relationship between the Band III and the lipid rafts, we treated the membranes by MβCD. Upon

the addition of 2 mM MβCD to get rid of the cholesterol-rich domains or lipid rafts, the height of the inner leaflet membrane decreased (shown in Figure 6C) and the recognition signals disappeared (shown in Figure 6D), indicating that the Band III was removed. Furthermore, there was no recognition signals to be resolved when scanning the inner leaflet of membranes with the bare or APTES modified tips (see Figure S1 in the Supporting Information). Altogether, these results reveal that cholesterol contributes significantly to the formation and stability of the protein domains, and the Band III may be an important protein of lipid rafts in the inner leaflet of erythrocyte membranes.

3. Discussion

The dynamic structure and characteristics of cell membranes at the molecular level are essential in biophysics and cell biology. Study of the molecular structure of lipid rafts would aid in eventually clarifying the mechanism of various membrane functions. Because of the limited approach to exploration of the heterogeneity and dynamic state of lipid rafts, the debate of whether lipid rafts exist still continues.[14,43,44]

The advantage of AFM is that it can image biological specimens with incredible resolution under physiological conditions without fixation and staining, so it has become a powerful tool in biological imaging and analysis. We prepared native erythrocyte membranes (Figures 1 and 2A) to replace the previously studied artificial membranes. We investigated the molecular determinants responsible for their insensitivity to Triton X-100 solubilization by AAC mode AFM. In AAC mode, the tip taps the sample gently and the lateral force is greatly diminished, so that it enables to obtain the reproducible images on the same area of the sample (Figure 4) and causes little damage to the sample (Figure 3). Moreover, time-lapse AFM can simultaneously probe the change of erythrocyte membranes induced by MβCD (Figures 2 and 5), which is not possible with electron microscopy due to the sample preparation requirement, such as fixation or freezing; as a result, the microdomains melted by MβCD in the in situ AFM images would represent the morphology of lipid rafts approximately.

Lipid rafts are dynamic microdomains (or nanoscale domains) enriched with sphingomyelin, cholesterol, and proteins;[43] therefore, direct observation of static membranes or microdomains by a high-resolution in situ technique is the most appropriate approach to study the transient morphology of lipid rafts. In addition, our experiments were performed at room temperature (about 23 °C), by which most of lipid rafts may be kept and no phase separation can occur, according to reported results from fluorometry experiments indicating that there are lipid rafts in erythrocyte membranes at 4, 23, and 37 °C.[45]

Membrane lateral heterogeneity is very important to the function of biological membranes, which is supported by the concept of lipid rafts.[36] In contrast to the traditional membrane model, our previous findings by in situ AFM reveal that the outer and inner leaflet of the erythrocyte membranes differ greatly.[32] The outer leaflet membrane is smooth and flat (Figure 1A), whereas the inner leaflet membrane is rough with a high areal density of the embedded proteins (Figure 1B). The outer and inner leaflet membranes experience different effects when treated with MβCD (Figure 2). The outer leaflet membrane is more sensitive to MβCD, while the inner leaflet membrane is more stable. After most of the proteins in the inner leaflet membrane are digested by trypsin, the inner leaflet becomes fragile, and the membrane morphology treated with MβCD is similar to that of the outer leaflet membrane treated with MβCD (Figure 3). These results reveal that the proteins, such as the Band III, may play an important role in the maintenance of both morphology and function of cell membranes.[46] Meanwhile, protein–lipid and protein–protein interactions could be equally important in the formation, maintenance, and dynamics of these membrane domains (Figure 2 to 5).

In situ and direct observation of the DRMs at high resolution is an alternative approach to positively study the lipid rafts. In our experiment, the DRMs were prepared only by the extraction of erythrocytes membranes with 0.1% (v/v) Triton X-100 at 4 °C and the conditions were much more moderate than those of traditional methods, so the structure and properties of DRMs were retained fairly well. For the first time, we directly confirm the existence of DRMs in native erythrocyte membranes in a real-time manner (Figure 4A).

The DRMs from the outer and inner leaflets of membranes are quite different (Figure 5A), which indicates that Triton X-100 had different effects on the different leaflets of cell membranes. One possible reason may be that the membrane proteins could play an important role in the morphology maintenance of lipid rafts. Meanwhile, the interaction of cell membranes with the mica surface may contribute to these phenomena. While the lipid bilayer was on the top of membrane proteins, the detergent and MβCD interacted with the lipid bilayer intensively. However, when the inner leaflet membrane faced up, the situation reversed; the lipid bilayer is under the proteins and tightly attached onto the mica surface, so that the detergent and MβCD might have less effect on the lipid bilayer (Figures 2 and 5). After the proteins in the inner leaflet were digested by trypsin, the lipid bilayer was exposed and the inner leaflet interacted with MβCD as quickly and intensively as the outer leaflet membrane (Figure 3).

Lipid rafts ought to be defined by their functions instead of by the method used to isolate them. The hypothesis of lipid rafts indicates that lipid rafts execute functions through the raft proteins; for example, the clathrin and caveolin in lipid rafts mediate the endocytosis.[6,47,48] The relationship between the erythrocyte anion transporter, the Band III, and lipid rafts was studied in this work. Our findings, based on the molecular recognition technique, show that the Band III is localized in the lipid raft domains (Figure 6). As reported previously, the Band III is not only the anion transporter but also connects with the skeleton of cell membranes, such as ankyrin and spectrin, to help maintaining the mechanical properties and integrity of the erythrocytes.[46] Our results provide direct proof that lipid rafts are functional domains.

It should be noted that the DRMs may not represent the whole of lipid rafts, and the compositions of the DRMs

small NANO MICRO

do not completely coincide with those of lipid rafts. Many questions about lipid rafts are not resolved as yet. This work only discloses some characteristics of lipid rafts; more work to further reveal their nature is still required.

4. Conclusion

We used in situ AFM to observe erythrocyte membranes treated with MβCD and Triton X-100, and confirmed the existence of lipid rafts. Based on the AFM images, we deduce that the sizes and shapes of lipid rafts are stochastic. The sizes of lipid rafts are mostly in the range 100 to 300 nm. The outer and inner leaflets of the membranes are different in respect to both morphology and behavior when treated with MβCD. Membrane proteins play important roles in the maintenance of lipid rafts, and the Band III may be a key protein in lipid rafts. Our studies are important to reveal the actual structure of cell membranes, and the functions of lipid rafts (e.g., signal transduction and virus infections). These results would pave the way for further study of lipid rafts in nucleated somatic cells.

5. Experimental Section

Preparation of Aminopropyltriethoxysilane (APTES)-Mica Substrate: APTES-mica substrate was prepared as described elsewhere.[49] Briefly, a desiccator was purged with argon for 2 min, and then 30 µL APTES (99% purity, Sigma-Aldrich, St. Louis, MO) and 10 µL ***N,N***-diisopropylethylamine (99% purity, Sigma-Aldrich, St. Louis, MO) were respectively injected into the small containers at the bottom of the desiccator respectively. Subsequently, the desiccator was purged with argon for 2 min. Mica sheets were stripped and placed in the desiccator, and then the desiccator was sealed off after purging for 3 min, leaving the mica exposed to the APTES vapor for 1 h. Finally, the containers were removed, and the desiccator was purged again. The treated mica (APTES-mica) was stored in the sealed desiccator for use.

Preparation of Erythrocyte Membranes: Erythrocyte membranes were prepared as described elsewhere.[22] To prepare human erythrocytes, two drops of fresh human blood from the AFM operator in our lab (no formal consent and no IRB approval was necessary, because the AFM operator did agree to donate the blood for the experiment and the volume drawn was less than 0.05 mL) were washed five times with 1 mL phosphate buffered saline (PBS; 136.9 mM NaCl, 2.7 mM KCl, 1.5 mM KH_2PO_4, 8.1 mM $Na_2HPO_4{\cdot}7H_2O$, pH 7.4). 200 µL dilute solution of the washed erythrocytes was deposited on the APTES-mica substrate and was allowed to adhere to the substrate for about 20 min. To obtain the outer membrane, flat erythrocyte ghosts – erythrocytes attached to APTES-mica – were sheared open by a slow stream of hypotonic buffer solution (6.845 mM NaCl, 0.135 mM KCl, 0.075 mM KH_2PO_4, 0.405 mM $Na_2HPO_4{\cdot}7H_2O$, pH 7.4) through a needle at an angle of 20°. To obtain the inner membrane without skeleton proteins in one-step preparation, erythrocytes were sheared open by a fast stream of hypotonic buffer solution through a needle at an angle of 20°. The prepared erythrocyte membranes were imaged by AFM in PBS immediately.

Digestion of the Inner Leaflet of Cell Membranes: The washed erythrocytes were sheared open by the fast hypotonic solution as described above. The prepared membranes were digested by trypsin (Sigma-Aldrich, St. Louis, MO; 1 mg mL^{-1} in PBS, 345 U mg^{-1}) for 1 h at 37 °C. Then, the membranes were washed in PBS three times for imaging. After recording the images, 2 mM MβCD was injected into the AFM sample chamber to track the membrane changes.

Preparation of DRMs: Erythrocyte membranes were prepared as described above, and then 200 µL 0.1% (v/v) Triton X-100 (diluted in PBS, pH 7.4) solution was deposited on the membranes for 4 min at 4 °C. The sample was rinsed with PBS three times to remove the remaining Triton X-100. The DRMs of erythrocytes were scanned in PBS. After recording DRMs images, 2 mM MβCD (Sigma-Aldrich, St. Louis, MO.) was injected into the AFM sample chamber to continuously scan the same area under the same conditions.

AFM Imaging: Erythrocyte membranes and DRMs were imaged by AFM 5500 (Agilent Technologies, Chandler, AZ) equipped with an 80 µm × 80 µm scanner. Topographic images were recorded in AAC mode using oxide-sharpened microfabricated Si_3N_4 cantilevers (Microlevers, Veeco Metrology LLC, Santa Barbara, CA) with a spring constant of 0.01 Nm^{-1} and at a scanning speed of 1.5–1.7 Hz. Images were obtained at room temperature (21–25 °C) in PBS. All images were recorded as 512 × 512 pixels. The size and height of the DRMs were measured by PicoScan 5.3.3 software (Agilent Technologies, Chandler, AZ).

AFM Recognition Imaging: Silicon-nitride cantilever tips (Microlever, Veeco, Santa Barbara, CA, coated for MacMode AFM by Agilent Technologies, Chandler, AZ) for recognition imaging were modified as described elsewhere.[22] Briefly, anti-Band III antibodies (Abcam, catalog no. ab55830) were reacted with ***N***-succinimidyl-3-(acetylthio) propionate (SATP, Sigma inc.) and purified in a PD-10 column (Amersham Pharmacia Biotech). The cantilevers were cleaned in a UV cleaner, treated with APTES vapor, and then reacted with PEG crosslinker (MaL-PEG2000-NHS, JenKem Technology Co., Ltd., Beijing) using triethylamine and $CHCl_3$. The SATP-labeled antibodies were bound to the PEG crosslinkers with NH_2OH (Sigma) in PBS. The tips were then rinsed in PBS and stored at 4 °C until use. Recognition imaging was performed in Magnetic AC (MAC) mode AFM 5500 with a PicoTREC recognition imaging attachment (Agilent Technologies, Chandler, AZ). Topographic and recognition images were acquired simultaneously as 512 × 512 pixels, and the scan rates were 1 Hz.

Supporting Information

Supporting Information is available from the Wiley Online Library or from the author.

Acknowledgements

This work was supported by MOST (grant no. 2011CB933600, to HW), NSFC (Grant no. 21073181 and no. 20975098, to HW) and the "100 talent Program" of CAS (to HW).

[1] S. J. Singer, G. L. Nicolson, *Science* **1972**, *175*, 720.
[2] H. J. Galla, E. Sackmann, *J. Am. Chem. Soc.* **1975**, *97*, 4114.
[3] K. Simons, E. Ikonen, *Nature* **1997**, *387*, 569.
[4] D. A. Brown, E. London, *J. Biol. Chem.* **2000**, *275*, 17221.
[5] D. A. Brown, *Physiology* **2006**, *21*, 430.
[6] K. Simons, D. Toomre, *Nat. Rev. Mol. Cell Biol.* **2000**, *1*, 31.
[7] L. Rajendran, K. Simons, *J. Cell Sci.* **2005**, *118*, 1099.
[8] D. R. Taylor, N. M. Hooper, *Mol. Membr. Biol.* **2006**, *23*, 89.
[9] H. Wang, P. Yang, K. Liu, F. Guo, Y. Zhang, G. Zhang, C. Jiang, *Cell Res.* **2008**, *18*, 290.
[10] G. R. Chichili, W. Rodgers, *Cell Mol. Life Sci.* **2009**, *66*, 2319.
[11] S. Schuck, M. Honsho, K. Ekroos, A. Shevchenko, K. Simons, *Proc. Natl. Acad. Sci. USA* **2003**, *100*, 5795.
[12] D. Lingwood, K. Simons, *Nat. Protoc.* **2007**, *2*, 2159.
[13] L. J. Pike, *Biochem. J.* **2004**, *378*, 281.
[14] S. Munro, *Cell* **2003**, *115*, 377.
[15] T. K. Kerppola, *Nat. Rev. Mol. Cell Biol.* **2006***7*, 449.
[16] K. Cottingham, *Anal. Chem.* **2004**, *76*, 403A.
[17] C. Dietrich, L. A. Bagatolli, Z. N. Volovyk, N. L. Thompson, M. Levi, K. Jacobson, E. Gratton, *Biophys. J.* **2001**, *80*, 1417.
[18] K. El Kirat, S. Morandat, *Biochim. Biophys. Acta, Biomembr.* **2007**, *1768*, 2300.
[19] A. S. Shaw, *Nat. Immunol.* **2006**, *7*, 1139.
[20] G. van Meer, D. R. Voelker, G. W. Feigenson, *Nat. Rev. Mol. Cell Biol.* **2008**, *9*, 112.
[21] C. Eggeling, C. Ringemann, R. Medda, G. Schwarzmann, K. Sandhoff, S. Polyakova, V. N. Belov, B. Hein, C. von Middendorff, A. Schonle, S. W. Hell, *Nature* **2009**, *457*, 1159.
[22] J. G. Jiang, X. Hao, M. J. Cai, Y. P. Shan, X. Shang, Z. Y. Tang, H. D. Wang, *Nano Lett.* **2009**, *9*, 4489.
[23] G. Andre, S. Kulakauskas, M.P. Chapot-Chartier, B. Navet, M. Deghorain, E. Bernard, P. Hols, Y. F. Dufrene, *Nat. Commun.* **2010**, *1*.
[24] D. J. Muller, *Biochemistry* **2008**, *47*, 7986.
[25] P. Hinterdorfer, Y. F. Dufrene, *Nat. Methods* **2006**, *3*, 347.
[26] D. J. Muller, Y. F. Dufrene, *Nat. Nanotechnol.* **2008**, *3*, 261.
[27] S. Morandat, K. El Kirat, *Langmuir* **2006**, *22*, 5786.
[28] M. C. Giocondi, V. Vie, E. Lesniewska, J. P. Goudonnet, C. Le Grimellec, *J. Struct. Biol.* **2000**, *131*, 38.
[29] S. C. Murphy, B. U. Samuel, T. Harrison, K. D. Speicher, D. W. Speicher, M. E. Reid, R. Proaska, P. S. Low, M. J. Tanner, N. Mohandas, K. Haldar, *Blood* **2004**, *103*, 1920.
[30] C. Crepaldi Domingues, A. Ciana, A. Buttafava, C. Balduini, E. de Paula, G. Minetti, *J. Membr. Biol.* **2009**, *227*, 39.
[31] A. H. Swihart, J. M. Mikrut, J. B. Ketterson, R. C. MacDonald, *J. Microsc.* **2001**, *204*, 212.
[32] H. D. Wang,X. Hao, Y. P. Shan, J. G. Jiang, M. J. Cai, X. Shang, *Ultramicroscopy* **2010**, *110*, 305.
[33] K. Motoyama, H. Toyodome, R. Onodera, T. Irie, F. Hirayama, K. Uekama, H. Arima, *Biol. Pharm. Bull.* **2009**, *32*, 700.
[34] A. K. Kenworthy, B. J. Nichols, C. L. Remmert, G. M. Hendrix, M. Kumar, J. Zimmerberg, J. Lippincott-Schwartz, *J. Cell Biol.* **2004**, *165*, 735.
[35] C. Dietrich, Z. N. Volovyk, M. Levi, N. L. Thompson, K. Jacobson, *Proc. Natl. Acad. Sci. USA* **2001**, *98*, 10642.
[36] K. Jacobson, O. G. Mouritsen, R. G. W. Anderson, *Nat. Cell Biol.* **2007**, *9*, 7.
[37] A. D. Dupuy, D. M. Engelman, *Proc. Natl. Acad. Sci. USA* **2008**, *105*, 2848.
[38] S. J. Johnson, T. M. Bayerl, D. C. McDermott, G. W. Adam, A. R. Rennie, R. K. Thomas, E. Sackmann, *Biophys. J.* **1991**, *59*, 289.
[39] R. Zidovetzki, I. Levitan, *Biochim. Biophys. Acta, Biomembr.* **2007**, *1768*, 1311.
[40] M. J. A. Tanner, *Mol. Membr. Biol.* **1997**, *14*, 155.
[41] P. Gane, C. Le Van Kim, V. Bony, W. El Nemer, I. Mouro, V. Nicolas, Y. Colin, J. P. Cartron, *Brit. J. Haematol.* **2001**, *113*, 680.
[42] Y. P. Shan, Z. Y. Wang, X. A. Hao, X. Shang, M. J. Cai, J. G. Jiang, X. X. Fang, H. D. Wang, Z. Y. Tang, *Anal. Methods* **2010**, *2*, 805.
[43] D. Lingwood, K. Simons, *Science* **2010**, *327*, 46.
[44] L. J. Pike, *J. Lipid Res.* **2009**, *50*, S323.
[45] I. Mikhalyov, A. Samsonov, *Biochim. Biophys. Acta, Biomembr.* **2011**, *1808*, 1930.
[46] L. L. Peters, R. A. Shivdasani, S. C. Liu, M. Hanspal, K. M. John, J. M. Gonzalez, C. Brugnara, B. Gwynn, N. Mohandas, S. L. Alper, S. H. Orkin, S. E. Lux, *Cell* **1996**, *86*, 917.
[47] Y. Z. Zheng, L. J. Foster, *J. Lipid Res.* **2009**, *50*, 1976.
[48] Y. Yao, S. Hong, H. Zhou, T. Yuan, R. Zeng, K. Liao, *Cell Res.* **2009**, *19*, 497.
[49] H. D. Wang, R. Bash, J. G. Yodh, G. L. Hager, D. Lohr, S. M. Lindsay, *Biophys. J.* **2002**, *83*, 3619.

Received: October 16, 2011
Published online: February 20, 2012

